

Joint Near-Field Sensing and Visibility Region Detection with Extremely Large Aperture Arrays

Huiping Huang^{*}, Alireza Pourafzal^{*}, Hui Chen^{*}, Musa Furkan Keskin^{*}, Mengting Li^{†,*},
Yu Ge^{*}, Fredrik Tufvesson[‡], Henk Wymeersch^{*}, Xuesong Cai^{§,‡}

^{*}Chalmers University of Technology [†]Aalborg University [‡]Lund University [§]Peking University

Abstract—In this paper, we consider near-field localization and sensing with an extremely large aperture array under partial blockage of array antennas, where spherical wavefront and spatial non-stationarity are accounted for. We propose an Ising model to characterize the clustered sparsity feature of the blockage pattern, develop an algorithm based on alternating optimization for joint channel parameter estimation and visibility region detection, and further estimate the locations of the user and environmental scatterers. The simulation results confirm the effectiveness of the proposed algorithm compared to conventional methods.

Index Terms—Extremely large aperture array, near-field channel estimation, visible region detection, partial blockage detection

I. INTRODUCTION

Sensing, in terms of estimating the state (e.g., position) of user equipment (UE) and environmental scatterers, is a key task in wireless networks, which highly overlaps with *channel estimation* in wireless communications [1]–[3]. Sensing (or channel estimation) is mostly based on the planar wavefront assumption in current and past generations of wireless systems [4], [5]. However, it faces serious challenges in future wireless systems, as the array size increases by an order of magnitude and the operating frequencies go to millimeter wave (mmWave) and Terahertz (THz) bands [6]–[9]. As a result, the near-field (NF) condition will become increasingly prevalent in various applications. In NF, the planar wavefront assumption is invalid, and instead, the spherical wavefront model should be considered. The spherical wavefront model accounts for angle and distance information, which is more complicated than the planar wavefront model. Additionally, the entire antenna array is affected by spatial non-stationary (SnS) due to the NF effect and partial blockage [10]–[13] (partial blockage is also referred to as visibility region (VR); see [14]–[19]).

To address the above challenges, various joint channel estimation and VR detection methods are proposed in the literature [14]–[24]. These works characterize the NF channel response as a product of channel gain, indicator factor, and NF steering vector, and can be categorized into deterministic, stochastic, and hybrid channel models. Deterministic models used in [14]–[18] are site-specific and they determine the indicator factor as either 0 or 1, while defining the steering vector as a function of angle and distance. Stochastic models

are used in [19]–[21] and describe the indicator factor using statistical parameters without explicitly modeling the physical environment. For hybrid models used in [22]–[24], the indicator factor is statistically determined as 0 or 1, and the steering vector is a function of angle and distance. The deterministic models and hybrid models are more preferred for positioning and mapping, as the stochastic models do not explicitly capture angle and distance information. Note that all existing studies assume that antenna elements obstructed by blockage (i.e., outside the line-of-sight region) do not contribute to the array’s channel response. However, this assumption is practically not true due to the diffraction and penetration effects of obstacles, which have been verified by measurement data as in [10]–[13].

From the methodology perspective, existing methods can be classified into two groups: non-Bayesian inference [14]–[18] and Bayesian inference [19]–[24]. To be specific, non-Bayesian inference methods treat joint channel estimation and VR detection as compressive sensing problems, and solve them by orthogonal matching pursuit [14], [17], [18], maximum likelihood estimation (MLE) [15]–[17], and/or alternating direction method of multipliers [18]. These non-Bayesian inference methods [14]–[18] and one Bayesian inference method [24] rely on the subarrays, which assume that the subchannel of each subarray can be treated as spatial stationary. However, this assumption may not be practical, especially when there exists partial blockages. For the remaining Bayesian inference methods, [19] and [21] adopt the Dirichlet process and Bernoulli-Gaussian distribution to model the VR indicator factor, respectively, which fail to characterize the clustered sparsity of the VR indicator vector; while [20], [22], and [23] employ nested Bernoulli-Gaussian distribution, three-layer hidden Markov chain, and one-order Markov chain, respectively, to describe the clustered sparsity of the indicator vector. These Markov chains are complicated in terms of modeling the clustered sparsity.

In this paper, we propose a new channel model in partial blockage scenario and an algorithm for joint channel estimation and VR detection. Our main contributions include: (i) We develop a simpler model, i.e., the *Ising* model, to capture the clustered sparsity of the indicator vector. (ii) To account for the data from [10]–[13], we model the channel response (when it is blocked) as a Gaussian distribution with small variance, which is essentially different from the literature [14]–[24]. (iii) We propose an alternating optimization (AO)-based algorithm for joint NF sensing and VR detection, which performs better than conventional methods, verified by simulations.

This paper is supported by the Vinnova B5GPOS Project under Grant 2022-01640, the HORIZON-MSCA through the project NEAT-6G under Grant 101152670, and the Swedish Research Council (VR) through the project 6G-PERCEF under Grant 2024-04390.

II. SIGNAL MODEL

We consider an uplink time division duplexing scenario, as shown in Fig. 1 (a), where multiple single-antenna UEs transmit orthogonal frequency division multiplexing (OFDM) pilot signals to a base station (BS) equipped with a uniform linear array (ULA) consisting of $N \gg 1$ half-wavelength spaced antennas. Since different UEs adopt orthogonal pilot sequences during the channel estimation stage, an arbitrary UE is considered in the following sections. The pilot signals contain K subcarriers and T symbols. There are obstacles between the extremely large aperture array (ELAA) and the UE, which partially block the ELAA. The channel response at the reference point (center point of the ELAA) contributed by the l -th path reads [10]

$$x_k^{(l)} = g^{(l)} e^{-j2\pi f_k (d^{(l)} + d_{\text{UE}}^{(l)})/c}, \quad l = 0, 1, \dots, L-1, \quad (1)$$

where L denotes the total number of paths (assumed to be known in this paper), $g^{(l)}$ is the complex channel gain, $f_k = f_c + k\Delta_f$ with f_c being the carrier frequency and Δ_f being the subcarrier spacing, $d^{(l)}$ denotes the distance between the l -th scatterer and the reference point, $d_{\text{UE}}^{(l)}$ denotes the propagation distance from the UE to the l -th scatterer ($d_{\text{UE}}^{(0)} = 0$ for line-of-sight (LoS)), and c is the speed of light. Then, the channel response of the n -th antenna at the k -th subcarrier and t -th snapshot, contributed by the l -th path, is given as

$$x_{n,k}^{(l)} = \alpha_n^{(l)} x_k^{(l)} \frac{d^{(l)}}{d_n^{(l)}} e^{j2\pi f_k (d^{(l)} - d_n^{(l)})/c} \quad (2a)$$

$$= \alpha_n^{(l)} g^{(l)} \frac{d^{(l)}}{d_n^{(l)}} e^{-j2\pi f_k d_n^{(l)}/c} e^{-j2\pi f_k d_{\text{UE}}^{(l)}/c}, \quad (2b)$$

where $\alpha_n^{(l)}$ denotes a stochastic variable characterizing the SnS effect, and $d_n^{(l)} = \sqrt{(d^{(l)})^2 - 2d^{(l)}\delta_n\Delta \sin(\theta^{(l)}) + \delta_n^2\Delta^2}$ is the distance between the l -th scatterer and the n -th antenna, with $\theta^{(l)}$ being the angle of arrival (AoA) of the l -th path, Δ being the element-spacing, and $\delta_n = \frac{2n-N-1}{2}$ for $n = 1, 2, \dots, N$. The relation between the position of the l -th scatterer and its channel parameters is shown in Fig. 1 (b).

Stacking $x_{n,k}^{(l)}$ for $n = 1, 2, \dots, N$, into a column vector $\mathbf{x}_k^{(l)} \in \mathbb{C}^N$, we obtain $\mathbf{x}_k^{(l)} = g^{(l)} \boldsymbol{\alpha}^{(l)} \odot \mathbf{h}_k^{(l)}$, where \odot denotes the Hadamard (entry-wise) product, $\boldsymbol{\alpha}^{(l)} \triangleq [\alpha_1^{(l)}, \alpha_2^{(l)}, \dots, \alpha_N^{(l)}]^T \in \mathbb{C}^N$, and $\mathbf{h}_k^{(l)} \in \mathbb{C}^N$ is defined as

$$\mathbf{h}_k^{(l)} = e^{-j2\pi f_k d_{\text{UE}}^{(l)}/c} \begin{bmatrix} \frac{d^{(l)}}{d_1^{(l)}} e^{-j2\pi f_k d_1^{(l)}/c}, \dots, \frac{d^{(l)}}{d_N^{(l)}} e^{-j2\pi f_k d_N^{(l)}/c} \end{bmatrix}^T. \quad (3)$$

The observation data of the ELAA at the k -th subcarrier and t -th snapshot, denoted by $\mathbf{y}_k \in \mathbb{C}^N$, can be given as

$$\mathbf{y}_{k,t} = \left(\sum_{l=0}^{L-1} \mathbf{x}_k^{(l)} \right) s_{k,t} + \mathbf{n}_{k,t}, \quad (4)$$

where $s_{k,t}$ is the pilot signal (which is equal to 1 without loss of generality), and $\mathbf{n}_{k,t} \in \mathbb{C}^N \sim \mathcal{CN}(\mathbf{0}, \sigma_n^2 \mathbf{I})$ with σ_n^2 denoting the noise variance. Stacking (based on different stacking manners) $\mathbf{y}_{k,t}$ for all k and t , we obtain

$$\check{\mathbf{y}} = \check{\mathbf{R}} \boldsymbol{\alpha} + \check{\mathbf{n}}, \quad \tilde{\mathbf{y}} = \tilde{\mathbf{R}} \mathbf{h} + \tilde{\mathbf{n}}, \quad \bar{\mathbf{y}} = \bar{\mathbf{R}} \mathbf{g} + \bar{\mathbf{n}}, \quad (5)$$

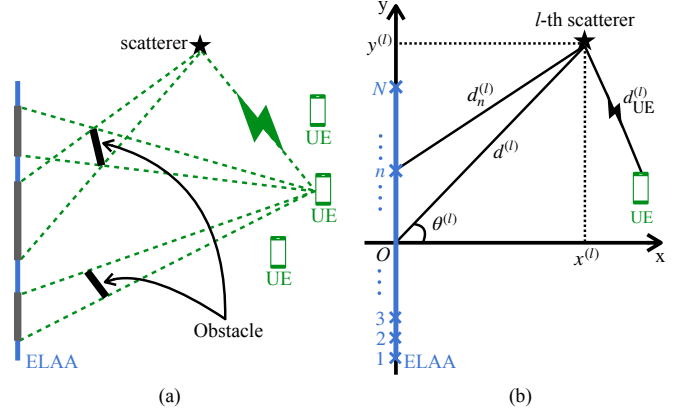


Fig. 1: (a) Illustration of near-field multipath (i.e., multiple scatterers) propagation in the presence of partial blockage. (b) Illustration of position of the l -th scatterer in the Cartesian coordinate system.

where the variables are defined in Appendix A.

III. PROPOSED MODEL AND METHOD

A. Proposed Model

We propose to model the antenna amplitude conditioned on the VR as

$$p(\boldsymbol{\alpha}^{(l)} | \mathbf{b}^{(l)}) = \prod_{n=1}^N p(\alpha_n^{(l)} | b_n^{(l)}), \quad (6)$$

where $\mathbf{b}^{(l)} \triangleq [b_1^{(l)}, b_2^{(l)}, \dots, b_N^{(l)}]^T \in \mathbb{R}^N$, and $b_n^{(l)}$ indicating if the n -th antenna is in the VR of the l -th path, as

$$b_n^{(l)} = \begin{cases} 1, & \text{if } n\text{-th antenna lies in VR,} \\ 0, & \text{otherwise.} \end{cases} \quad (7)$$

In (6), the amplitude at each antenna is modeled as

$$p(\alpha_n^{(l)} | b_n^{(l)}) = (1 - b_n^{(l)}) \mathcal{CN}(0, \sigma_b^2) + b_n^{(l)} \delta(\alpha_n - 1), \quad (8)$$

where σ_b^2 denotes the amplitude variance in the blockage region, and $\delta(\cdot)$ is the Dirac delta function. When the n -th antenna lies in the VR, then $b_n^{(l)} = 1$ and its amplitude follows $\delta(\alpha_n - 1)$, meaning that $\alpha_n = 1$ with probability one; otherwise, $b_n^{(l)} = 0$ and its amplitude follows $\mathcal{CN}(0, \sigma_b^2)$. Note that when $b_n^{(l)} = 1$ for all n and l , the observation reduces to $\mathbf{x}_k^{(l)} = g^{(l)} \mathbf{h}_k^{(l)}$, which corresponds to the general case of deterministic channel model without considering the SnS.

To proceed, we approximate the Dirac delta function by a complex Gaussian distribution with a very small variance σ_v^2 , and rewrite (8) as

$$p(\alpha_n^{(l)} | b_n^{(l)}) \approx (1 - b_n^{(l)}) \mathcal{CN}(0, \sigma_b^2) + b_n^{(l)} \mathcal{CN}(1, \sigma_v^2) \\ = \mathcal{CN}(b_n^{(l)}, (1 - b_n^{(l)}) \sigma_b^2 + b_n^{(l)} \sigma_v^2). \quad (9)$$

Since whether the antenna lies in the VR is related to its nearby antennas, we propose to utilize an *Ising model* (a standard type of Markov random fields [25]) to characterize the clustered sparsity of $\mathbf{b}^{(l)}$, which is given as

$$p(\mathbf{b}^{(l)}) = \frac{1}{A} e^{-\left(\sum_{(n,m) \in \mathcal{E}} \beta_{nm}^{(l)} b_n^{(l)} b_m^{(l)} + \sum_{n=1}^N \gamma_n^{(l)} b_n^{(l)} \right)}, \quad (10)$$

where $b_n^{(l)} \triangleq 2b_n^{(l)} - 1$ are substitution variables, \mathcal{E} is the set of edges representing neighboring antenna pairs, $\beta_{nm}^{(l)}$ denotes

the interaction strength between the n -th and m -th antennas, $\gamma_n^{(l)}$ is the individual strength parameter for the n -th antenna, and A is the normalization parameter. A detailed explanation of the proposed Ising model is given in Appendix B.

B. Proposed Method

The joint distribution based on (4) can be given by

$$p(\mathbf{y}, \{\boldsymbol{\alpha}^{(l)}\}, \{\mathbf{b}^{(l)}\}, \{\mathbf{g}^{(l)}\}; \{\theta^{(l)}\}, \{d^{(l)}\}, \{d_{\text{UE}}^{(l)}\}) \\ = p(\mathbf{y} | \{\boldsymbol{\alpha}^{(l)}\}, \{\mathbf{b}^{(l)}\}, \{\mathbf{g}^{(l)}\}; \{\theta^{(l)}\}, \{d^{(l)}\}, \{d_{\text{UE}}^{(l)}\}) \prod_{l=0}^{L-1} p(\boldsymbol{\alpha}^{(l)} | \mathbf{b}^{(l)}) p(\mathbf{b}^{(l)}), \quad (11)$$

where $p(\mathbf{y} | \{\boldsymbol{\alpha}^{(l)}\}, \{\mathbf{b}^{(l)}\}, \{\mathbf{g}^{(l)}\}; \{\theta^{(l)}\}, \{d^{(l)}\}, \{d_{\text{UE}}^{(l)}\}) = \mathcal{CN}(\sum_{l=0}^{L-1} \mathbf{x}^{(l)}, \sigma_n^2 \mathbf{I})$. Substituting the results in (6), (9) and (10) into (11) yields the negative log-likelihood function, $-\log p(\mathbf{y}, \{\boldsymbol{\alpha}^{(l)}\}, \{\mathbf{b}^{(l)}\}, \{\mathbf{g}^{(l)}\}; \{\theta^{(l)}\}, \{d^{(l)}\}, \{d_{\text{UE}}^{(l)}\}) = f_1 + f_2 + f_3 + L \log A$, where

$$f_1 \triangleq \frac{1}{\sigma_n^2} \|\mathbf{y} - \mathbf{R}\mathbf{w}\|_2^2, \quad (12a)$$

$$f_2 \triangleq \sum_{l=0}^{L-1} \sum_{n=1}^N \frac{(\alpha_n^{(l)} - b_n^{(l)})^2}{(1 - b_n^{(l)})\sigma_b^2 + b_n^{(l)}\sigma_v^2}, \quad (12b)$$

$$f_3 \triangleq \sum_{l=0}^{L-1} \left(\sum_{(n,m) \in \mathcal{E}} \beta_{nm}^{(l)} b_n^{(l)} b_m^{(l)} + \sum_{n=1}^N \gamma_n^{(l)} b_n^{(l)} \right), \quad (12c)$$

and $L \log A$ is unrelated to the unknown channel parameters $\{\theta^{(l)}, d^{(l)}, d_{\text{UE}}^{(l)}, g^{(l)}, \alpha^{(l)}\}$ and the VR indicator vectors $\{\mathbf{b}^{(l)}\}$. In addition, \mathbf{y} , \mathbf{R} , and \mathbf{w} in (12a) equal to $\tilde{\mathbf{y}}$, $\tilde{\mathbf{R}}$, and $\boldsymbol{\alpha}$, respectively, when the first model in (5) is considered; \mathbf{y} , \mathbf{R} , and \mathbf{w} equal to $\tilde{\mathbf{y}}$, $\tilde{\mathbf{R}}$, and \mathbf{h} , respectively, when the second model in (5) is considered; and \mathbf{y} , \mathbf{R} , and \mathbf{w} equal to $\bar{\mathbf{y}}$, $\bar{\mathbf{R}}$, and \mathbf{g} , respectively, when the third model in (5) is considered. Consequently, the estimates of channel parameters and VR indicator vectors can be obtained via

$$\{\{\hat{\theta}^{(l)}\}, \{\hat{d}^{(l)}\}, \{\hat{d}_{\text{UE}}^{(l)}\}, \{\hat{g}^{(l)}\}, \{\hat{\boldsymbol{\alpha}}^{(l)}\}, \{\hat{\mathbf{b}}^{(l)}\}\} = \arg \min f_1 + f_2 + f_3. \quad (13)$$

The hyperparameters of the Ising model can be estimated by measurement data, and the estimations of channel parameters, VR indicator vector, and positions of all scatterers are presented as follows.

1) Estimation of Channel Parameters and VR Indicator:

By introducing the following auxiliary variables defined as:

$$\mathbf{b} \triangleq \mathbf{1}_T \otimes \left[(\mathbf{b}^{(0)})^T, (\mathbf{b}^{(1)})^T, \dots, (\mathbf{b}^{(L-1)})^T \right]^T \in \mathbb{R}^{NLT \times 1} \\ \mathbf{b}' \triangleq 2\mathbf{b} - \mathbf{1}_{NLT} \in \{-1, 1\}^{NLT \times 1}, \\ \mathbf{q} \triangleq \sigma_b^2 \mathbf{1}_{NLT} + (\sigma_v^2 - \sigma_b^2) \mathbf{b} \in \mathbb{R}^{NLT \times 1}, \\ \mathbf{Q} \triangleq \text{diag}(\mathbf{q}) \in \mathbb{R}^{NLT \times NLT}, \\ \tilde{\mathbf{E}}^{(l)} \triangleq \begin{bmatrix} 0 & \beta_{12}^{(l)} & \dots & \beta_{1N}^{(l)} \\ \beta_{21}^{(l)} & 0 & \dots & \beta_{2N}^{(l)} \\ \vdots & \vdots & \ddots & \vdots \\ \beta_{N1}^{(l)} & \beta_{N2}^{(l)} & \dots & 0 \end{bmatrix} \in \mathbb{R}^{N \times N}, \\ \mathbf{E} \triangleq \mathbf{I}_T \otimes \text{blkdiag}(\tilde{\mathbf{E}}^{(0)}, \tilde{\mathbf{E}}^{(1)}, \dots, \tilde{\mathbf{E}}^{(L-1)}) \in \mathbb{R}^{NLT \times NLT},$$

$$\tilde{\boldsymbol{\gamma}}^{(l)} \triangleq \left[\gamma_1^{(l)}, \gamma_2^{(l)}, \dots, \gamma_N^{(l)} \right]^T \in \mathbb{R}^{N \times 1},$$

$$\boldsymbol{\gamma} \triangleq \mathbf{1}_T \otimes \left[(\tilde{\boldsymbol{\gamma}}^{(0)})^T, (\tilde{\boldsymbol{\gamma}}^{(1)})^T, \dots, (\tilde{\boldsymbol{\gamma}}^{(L-1)})^T \right]^T \in \mathbb{R}^{NLT \times 1},$$

we reformulate: $f_1 = \frac{1}{\sigma_n^2} \|\mathbf{y} - \mathbf{R}\mathbf{w}\|_2^2$, $f_2 = \|\mathbf{Q}^{-\frac{1}{2}}(\boldsymbol{\alpha} - \mathbf{b})\|_2^2$, and $f_3 = \frac{1}{2} \mathbf{b}'^T \mathbf{E} \mathbf{b}' + \boldsymbol{\gamma}^T \mathbf{b}'$. Problem (13) is solved by the following two-step strategy:

$$\text{Step 1: } \{\hat{\mathbf{g}}, \hat{\mathbf{h}}, \hat{\boldsymbol{\alpha}}, \hat{\mathbf{b}}\} = \arg \min_{\{\mathbf{g}, \mathbf{h}, \boldsymbol{\alpha}, \mathbf{b}\}} f_1 + f_2 + f_3 \quad \text{s.t. } \mathbf{b} \in \{0, 1\}^{NLT}, \quad (14)$$

$$\text{Step 2: } \{\{\hat{\theta}^{(l)}\}, \{\hat{d}^{(l)}\}, \{\hat{d}_{\text{UE}}^{(l)}\}\} \leftarrow \hat{\mathbf{h}}, \quad \hat{\boldsymbol{\alpha}}^{(l)} = [\hat{\boldsymbol{\alpha}}]_{t, (l-1)N+1:lN}, \\ \hat{g}^{(l)} = [\hat{\mathbf{g}}]_l, \quad \hat{\mathbf{b}}^{(l)} = \left[\hat{\mathbf{b}} \right]_{(l-1)N+1:lN}. \quad (15)$$

Solve (14): Parameters \mathbf{g} , \mathbf{h} , $\boldsymbol{\alpha}$, and \mathbf{b} can be estimated under the AO framework.

- Estimate \mathbf{g} : Given $\bar{\mathbf{y}}$ and $\bar{\mathbf{R}}$ defined in (22) and (23a), respectively, the least squares (LS) solution for $\min_{\mathbf{g}} \|\bar{\mathbf{y}} - \bar{\mathbf{R}}\mathbf{g}\|_2^2$ can be expressed as $\hat{\mathbf{g}} = (\bar{\mathbf{R}}^H \bar{\mathbf{R}})^{-1} \bar{\mathbf{R}}^H \bar{\mathbf{y}}$.
- Estimate \mathbf{h} : Given $\tilde{\mathbf{y}}$ and $\tilde{\mathbf{R}}$ defined in (20) and (21a), respectively, the LS solution for $\min_{\mathbf{h}} \|\tilde{\mathbf{y}} - \tilde{\mathbf{R}}\mathbf{h}\|_2^2$ can be expressed as $\hat{\mathbf{h}} = (\tilde{\mathbf{R}}^H \tilde{\mathbf{R}})^{-1} \tilde{\mathbf{R}}^H \tilde{\mathbf{y}}$.
- Estimate $\boldsymbol{\alpha}$: To solve $\min_{\boldsymbol{\alpha}} \|\tilde{\mathbf{y}} - \tilde{\mathbf{R}}\boldsymbol{\alpha}\|_2^2$ with $\tilde{\mathbf{y}}$ and $\tilde{\mathbf{R}}$ defined in (18) and (19a), respectively, the linear minimum mean square error (LMMSE) estimator is adopted. The solution can be expressed as $\hat{\boldsymbol{\alpha}} = \boldsymbol{\mu}_\alpha + \boldsymbol{\Sigma}_\alpha \tilde{\mathbf{R}}^H (\tilde{\mathbf{R}} \boldsymbol{\Sigma}_\alpha \tilde{\mathbf{R}}^H + \sigma_n^2 \mathbf{I})^{-1} (\tilde{\mathbf{y}} - \tilde{\mathbf{R}} \boldsymbol{\mu}_\alpha)$, where $\boldsymbol{\mu}_\alpha = \mathbf{b}$ and $\boldsymbol{\Sigma}_\alpha = \text{diag}(\sigma_b^2(1 - \mathbf{b}) + \sigma_v^2 \mathbf{b})$ according to (9).
- Estimate \mathbf{b} : The subproblem $\min_{\mathbf{b} \in \{0, 1\}^{NLT}} (\boldsymbol{\alpha} - \mathbf{b})^H \mathbf{Q}^{-1} (\boldsymbol{\alpha} - \mathbf{b}) + \frac{1}{2} \mathbf{b}'^T \mathbf{E} \mathbf{b}' + \boldsymbol{\gamma}^T \mathbf{b}'$ can be relaxed to an unconstrained binary quadratic programming as

$$\min_{\mathbf{b}} 2\mathbf{b}^T \mathbf{E} \mathbf{b} + \mathbf{r}^T \mathbf{b}, \quad \text{s.t. } \begin{cases} \mathbf{0} \preceq \mathbf{b} \preceq \mathbf{1}_{NLT}, \\ (\mathbf{I}_{NLT} - \text{diag}(\mathbf{b})) \mathbf{b} \preceq \boldsymbol{\eta}, \end{cases} \quad (16)$$

where $\boldsymbol{\eta} \in \mathbb{R}^{NLT}$ is predefined and $\mathbf{r} = \mathbf{r}_1 + \mathbf{r}_2 + \mathbf{r}_3$ with $\mathbf{r}_1 \triangleq \left[\frac{|\alpha_1 - 1|^2}{\sigma_v^2} - \frac{|\alpha_1|^2}{\sigma_b^2}, \dots, \frac{|\alpha_{NLT} - 1|^2}{\sigma_v^2} - \frac{|\alpha_{NLT}|^2}{\sigma_b^2} \right]^T$, $\mathbf{r}_2 \triangleq -2\mathbf{E}^T \mathbf{1}$, and $\mathbf{r}_3 \triangleq 2\boldsymbol{\gamma}$. This problem can be solved via numerical optimization solvers.

Solve (15): Channel gain, antenna amplitude, and VR for each path and snapshot can be estimated by (15). The distances

Algorithm 1 Proposed AO-Based Algorithm for Solving (14)

- 1: **Input:** \mathbf{y} ($\bar{\mathbf{y}}$, $\tilde{\mathbf{y}}$, and $\check{\mathbf{y}}$), \mathbf{E} , $\boldsymbol{\gamma}$, σ_n^2 , σ_b^2 , σ_v^2 , I , ϵ
 - 2: **Output:** $\mathbf{g}_{(i+1)}$, $\mathbf{h}_{(i+1)}$, $\boldsymbol{\alpha}_{(i+1)}$, $\mathbf{b}_{(i+1)}$
 - 3: **Initialize:** $\mathbf{g}_{(0)}$, $\mathbf{h}_{(0)}$, $\boldsymbol{\alpha}_{(0)}$, $\mathbf{b}_{(0)}$
 - 4: **for** $i = 0, 1, \dots, I$ **do**
 - 5: $\bar{\mathbf{R}} \leftarrow (23a)$, $\mathbf{g}_{(i+1)} = (\bar{\mathbf{R}}^H \bar{\mathbf{R}})^{-1} \bar{\mathbf{R}}^H \bar{\mathbf{y}}$
 - 6: $\tilde{\mathbf{R}} \leftarrow (21a)$, $\mathbf{h}_{(i+1)} = (\tilde{\mathbf{R}}^H \tilde{\mathbf{R}})^{-1} \tilde{\mathbf{R}}^H \tilde{\mathbf{y}}$
 - 7: $\check{\mathbf{R}} \leftarrow (19a)$, $\boldsymbol{\alpha}_{(i+1)} = \boldsymbol{\mu}_\alpha + \boldsymbol{\Sigma}_\alpha \check{\mathbf{R}}^H (\check{\mathbf{R}} \boldsymbol{\Sigma}_\alpha \check{\mathbf{R}}^H + \sigma_n^2 \mathbf{I})^{-1} (\check{\mathbf{y}} - \check{\mathbf{R}} \boldsymbol{\mu}_\alpha)$
 - 8: $\mathbf{b}_{(i+1)} \leftarrow (16)$
 - 9: **if** $\frac{|\text{Obj}_{(i+1)} - \text{Obj}_{(i)}|}{|\text{Obj}_{(i)}|} \leq \epsilon$ **then**
 - 10: **break**
 - 11: **end if**
 - 12: **end for**
-

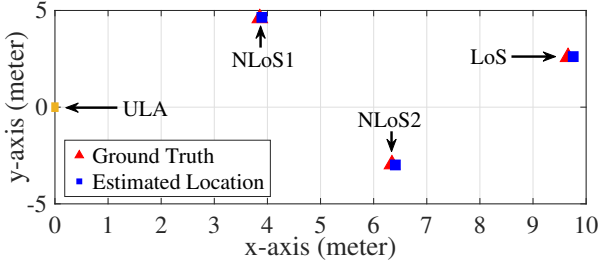


Fig. 2: Estimate of locations of $L = 3$ scatterers.

and AoA of each path can be estimated based on MLE using $\hat{\mathbf{h}}$ obtained from (14). To be specific, we extract $\hat{\mathbf{h}}_k^{(l)} \in \mathbb{C}^N$ for all K subcarriers from $\hat{\mathbf{h}}$. Then, we have

$$\left(\hat{d}_{\text{UE}}^{(l)}, \hat{d}^{(l)}, \hat{\theta}^{(l)} \right) = \arg \min_{d_{\text{UE}}, d, \theta} \sum_{k=1}^K \left\| \hat{\mathbf{h}}_k^{(l)} - \mathbf{h}_k(d_{\text{UE}}, d, \theta) \right\|_2^2, \quad (17)$$

where $\mathbf{h}_k(d_{\text{UE}}, d, \theta)$ is a function of d_{UE} , d , and θ as in (3).

2) *Estimation of Positions of UE and Scatterers:* After we obtain the estimates of distance and AoA of each path, the position of the l -th scatterer, i.e., $(\hat{x}^{(l)}, \hat{y}^{(l)})$, can be calculated as: $\hat{x}^{(l)} = \hat{d}^{(l)} \cos(\hat{\theta}^{(l)})$, $\hat{y}^{(l)} = \hat{d}^{(l)} \sin(\hat{\theta}^{(l)})$.

IV. SIMULATIONS

We consider a ULA of $N = 100$ antennas. A UE transmits OFDM signals, with carrier frequency being $f_c = 30$ GHz (i.e., wavelength $\lambda = 0.01$ m), $K = 4$ subcarriers, $T = 4$ snapshots, and bandwidth 2.88 MHz. The simulation parameters are compliant with 3GPP [26]. The ELAA element-spacing is set to be half of the wavelength, i.e., $\Delta = \frac{\lambda}{2} = 0.005$ m. The Fraunhofer distance is $d_F \triangleq \frac{2D^2}{\lambda} \approx 50$ m. We consider $L = 3$ paths, including one LoS and two non-line-of-sight (NLoS) paths. Other simulation parameters are given below.

- LoS: UE at $(d^{(0)}, \theta^{(0)}) = (10 \text{ m}, 15^\circ)$, and the antennas from index $\{75\}$ to index $\{80\}$ are blocked.
- NLoS1: The scatterer at $(d^{(1)}, \theta^{(1)}) = (6 \text{ m}, 50^\circ)$, and the antennas from index $\{11\}$ to index $\{14\}$ are blocked.
- NLoS2: The scatterer at $(d^{(2)}, \theta^{(2)}) = (7 \text{ m}, -25^\circ)$, and the antennas from index $\{34\}$ to index $\{38\}$ are blocked.

The estimated locations and ground truth of $L = 3$ scatterers are depicted in Fig. 2, which shows that the estimated locations are very close to the ground truth. The estimated VR are displayed in Fig. 3, showing that the proposed algorithm can detect all blocked antennas, and has false alarm for the two NLoS paths. The root mean squared error (RMSE) of location and channel gain versus signal-to-noise ratio (SNR) are plotted in Figs. 4 (left) and 4 (right), respectively. It is seen that the proposed method outperforms two LS-MLE-based methods, without considering the SnS and with random SnS, respectively. The LS-MLE-based method with known SnS is used as a benchmark, and the proposed method is slightly worse than it.

V. CONCLUSION

We investigated near-field localization and sensing with an extremely large aperture array (ELAA). We proposed an Ising

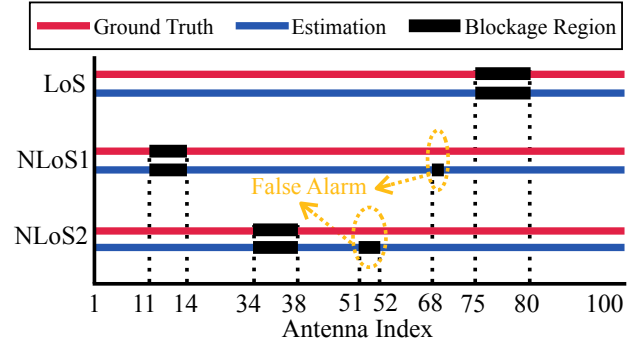


Fig. 3: Blockage region detection with SNR = 10 dB.

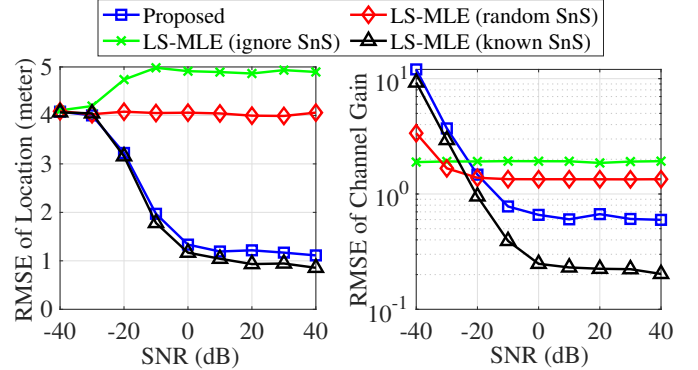


Fig. 4: RMSE of location (left) and channel gain (right) versus SNR.

model to characterize the clustered sparsity of the blockage pattern of ELAA and developed an alternating optimization-based algorithm for joint channel parameter estimation and visibility region detection. The simulation results indicated that the proposed algorithm achieves better performance than traditional methods.

APPENDIX A DERIVATION OF EQUATION (5)

We denote the realization of the SnS effect $\alpha_n^{(l)}$ at the t -th snapshot as $\alpha_{n,t}^{(l)}$, and define $\alpha_t^{(l)} \triangleq [\alpha_{1,t}^{(l)}, \alpha_{2,t}^{(l)}, \dots, \alpha_{N,t}^{(l)}]^T \in \mathbb{C}^N$. Inserting $\mathbf{x}_{k,t}^{(l)} = g^{(l)} \alpha_t^{(l)} \odot \mathbf{h}_k^{(l)}$ into (4) yields: $\mathbf{y}_{k,t} = (\mathbf{g}^T \otimes \mathbf{I}_N) \text{diag}(\alpha_t) \mathbf{h}_k + \mathbf{n}_{k,t}$, where \otimes is the Kronecker product, $\text{diag}(\cdot)$ generates a diagonal matrix with the argument as its main diagonal, and

$$\mathbf{g} \triangleq [g^{(0)}, g^{(1)}, \dots, g^{(L-1)}]^T \in \mathbb{C}^L,$$

$$\alpha_t \triangleq [(\alpha_t^{(0)})^T, (\alpha_t^{(1)})^T, \dots, (\alpha_t^{(L-1)})^T]^T \in \mathbb{C}^{NL},$$

$$\mathbf{h}_k \triangleq [(\mathbf{h}_k^{(0)})^T, (\mathbf{h}_k^{(1)})^T, \dots, (\mathbf{h}_k^{(L-1)})^T]^T \in \mathbb{C}^{NL}.$$

Stack $\mathbf{y}_{k,t}$ for all k into a matrix, as

$$\mathbf{Y}_t = (\mathbf{g}^T \otimes \mathbf{I}_N) \text{diag}(\alpha_t) [\mathbf{h}_1, \mathbf{h}_2, \dots, \mathbf{h}_K] + \mathbf{N}_t,$$

where $\mathbf{N}_t \triangleq [\mathbf{n}_{1,t}, \mathbf{n}_{2,t}, \dots, \mathbf{n}_{K,t}] \in \mathbb{C}^{N \times K}$. Vectorize \mathbf{Y}_t as $\mathbf{y}_t \triangleq \text{vec}(\mathbf{Y}_t) = ([\mathbf{h}_1, \mathbf{h}_2, \dots, \mathbf{h}_K]^T \otimes (\mathbf{g}^T \otimes \mathbf{I}_N)) \alpha_t + \mathbf{n}_t$, where \otimes denotes the Khatri-Rao product and $\mathbf{n}_t \triangleq \text{vec}(\mathbf{N}_t) \in \mathbb{C}^{NK}$. Stack \mathbf{y}_t for all t as a vector $\check{\mathbf{y}} \in \mathbb{C}^{NK T}$, as

$$\check{\mathbf{y}} \triangleq [\mathbf{y}_1^T, \mathbf{y}_2^T, \dots, \mathbf{y}_T^T]^T = \check{\mathbf{R}} \alpha + \check{\mathbf{n}}, \quad (18)$$

where

$$\tilde{\mathbf{R}} \triangleq \mathbf{I}_T \otimes ([\mathbf{h}_1, \dots, \mathbf{h}_K]^T \otimes (\mathbf{g}^T \otimes \mathbf{I}_N)) \in \mathbb{C}^{NKT \times NLT}, \quad (19a)$$

$$\boldsymbol{\alpha} \triangleq [\boldsymbol{\alpha}_1^T, \boldsymbol{\alpha}_2^T, \dots, \boldsymbol{\alpha}_T^T]^T \in \mathbb{C}^{NLT}, \quad (19b)$$

$$\tilde{\mathbf{n}} \triangleq [\mathbf{n}_1^T, \mathbf{n}_2^T, \dots, \mathbf{n}_T^T]^T \in \mathbb{C}^{NKT}. \quad (19c)$$

Inserting $\mathbf{x}_{k,t}^{(l)} = g^{(l)} \boldsymbol{\alpha}_t^{(l)} \odot \mathbf{h}_k^{(l)}$ into (4) yield: $\mathbf{y}_{k,t} = (\mathbf{g}^T \otimes \mathbf{I}_N) \text{diag}(\mathbf{h}_k) \boldsymbol{\alpha}_t + \mathbf{n}_{k,t}$. Stack $\mathbf{y}_{k,t}$ for all t into a matrix:

$$\mathbf{Y}_k = (\mathbf{g}^T \otimes \mathbf{I}_N) \text{diag}(\mathbf{h}_k) [\boldsymbol{\alpha}_1, \boldsymbol{\alpha}_2, \dots, \boldsymbol{\alpha}_T] + \mathbf{N}_k,$$

where $\mathbf{N}_k \triangleq [\mathbf{n}_{k,1}, \mathbf{n}_{k,2}, \dots, \mathbf{n}_{k,T}] \in \mathbb{C}^{N \times T}$. Vectorize \mathbf{Y}_k as $\mathbf{y}_k \triangleq \text{vec}(\mathbf{Y}_k) = ([\boldsymbol{\alpha}_1, \boldsymbol{\alpha}_2, \dots, \boldsymbol{\alpha}_T]^T \otimes (\mathbf{g}^T \otimes \mathbf{I}_N)) \mathbf{h}_k + \mathbf{n}_k$, with $\mathbf{n}_k \triangleq \text{vec}(\mathbf{N}_k) \in \mathbb{C}^{NT}$. Stack \mathbf{y}_k for all k as $\tilde{\mathbf{y}} \in \mathbb{C}^{NTK}$:

$$\tilde{\mathbf{y}} \triangleq [\mathbf{y}_1^T, \mathbf{y}_2^T, \dots, \mathbf{y}_K^T]^T = \tilde{\mathbf{R}} \mathbf{h} + \tilde{\mathbf{n}}, \quad (20)$$

where

$$\tilde{\mathbf{R}} \triangleq \mathbf{I}_K \otimes ([[\boldsymbol{\alpha}_1, \dots, \boldsymbol{\alpha}_T]^T \otimes (\mathbf{g}^T \otimes \mathbf{I}_N)]) \in \mathbb{C}^{NTK \times NLK}, \quad (21a)$$

$$\mathbf{h} \triangleq [\mathbf{h}_1^T, \mathbf{h}_2^T, \dots, \mathbf{h}_K^T]^T \in \mathbb{C}^{NLK}, \quad (21b)$$

$$\tilde{\mathbf{n}} \triangleq [\mathbf{n}_1^T, \mathbf{n}_2^T, \dots, \mathbf{n}_K^T]^T \in \mathbb{C}^{NTK}. \quad (21c)$$

Inserting $\mathbf{x}_{k,t}^{(l)} = g^{(l)} \boldsymbol{\alpha}_t^{(l)} \odot \mathbf{h}_k^{(l)}$ into (4) also yields: $\mathbf{y}_{k,t} = \mathbf{R}_{k,t} \mathbf{g} + \mathbf{n}_{k,t}$, where $\mathbf{R}_{k,t} \triangleq [\boldsymbol{\alpha}_t^{(0)}, \boldsymbol{\alpha}_t^{(1)}, \dots, \boldsymbol{\alpha}_t^{(L-1)}] \odot [\mathbf{h}_k^{(0)}, \mathbf{h}_k^{(1)}, \dots, \mathbf{h}_k^{(L-1)}]$. Stack $\mathbf{y}_{k,t}$ for all k and t as a vector $\tilde{\mathbf{y}} \in \mathbb{C}^{NKT}$, as

$$\tilde{\mathbf{y}} \triangleq [\mathbf{y}_{1,1}^T, \dots, \mathbf{y}_{1,T}^T, \dots, \mathbf{y}_{K,1}^T, \dots, \mathbf{y}_{K,T}^T]^T = \tilde{\mathbf{R}} \mathbf{g} + \tilde{\mathbf{n}}, \quad (22)$$

where

$$\tilde{\mathbf{R}} \triangleq [\mathbf{R}_{1,1}^T, \dots, \mathbf{R}_{1,T}^T, \dots, \mathbf{R}_{K,1}^T, \dots, \mathbf{R}_{K,T}^T]^T \in \mathbb{C}^{NKT \times L}, \quad (23a)$$

$$\mathbf{g} \triangleq [g^{(0)}, g^{(1)}, \dots, g^{(L-1)}]^T \in \mathbb{C}^L, \quad (23b)$$

$$\tilde{\mathbf{n}} \triangleq [\mathbf{n}_{1,1}^T, \dots, \mathbf{n}_{1,T}^T, \dots, \mathbf{n}_{K,1}^T, \dots, \mathbf{n}_{K,T}^T]^T \in \mathbb{C}^{NKT}. \quad (23c)$$

APPENDIX B

EXPLANATION OF THE ISING MODEL

First of all, the substitution variables b'_n are equal to either -1 or 1 , since $b_n = 0$ or 1 . We analyze the key components in the Ising model, i.e., $\beta_{nm} b'_n b'_m + \gamma_n b'_n + \gamma_m b'_m$, where we ignore the path index. Our goal is to minimize $\beta_{nm} b'_n b'_m + \gamma_n b'_n + \gamma_m b'_m$. Clearly, a negative β_{nm} will enforce $b'_n = b'_m = 1$ or $b'_n = b'_m = -1$; and a positive β_{nm} will enforce $(b'_n = 1 \text{ and } b'_m = -1)$ or $(b'_n = -1 \text{ and } b'_m = 1)$. On the other hand, a negative γ_n (reps. γ_m) will enforce $b'_n = 1$ (resp. $b'_m = 1$); while a positive γ_n (resp. γ_m) will enforce $b'_n = -1$ (resp. $b'_m = -1$). This indicates that the proposed Ising model can lead to clustered sparsity of \mathbf{b} due to the terms $\beta_{nm} b'_n b'_m$.

REFERENCES

- [1] H. Wymeersch, "A Fisher information analysis of joint localization and synchronization in near field," in *IEEE International Conference on Communications Workshops (ICC)*, Dublin, Ireland, 2020, pp. 1–6.
- [2] H. Chen, M. F. Keskin, A. Sakhnini, N. Decarli, S. Pollin, D. Dardari, and H. Wymeersch, "6G localization and sensing in the near field: Features, opportunities, and challenges," *IEEE Wireless Communications*, vol. 31, no. 4, pp. 260–267, 2024.
- [3] H. Gazzah and J. P. Delmas, "CRB-based design of linear antenna arrays for near-field source localization," *IEEE Transactions on Antennas and Propagation*, vol. 62, no. 4, pp. 1965–1974, 2014.
- [4] B. Friedlander, "Localization of signals in the near-field of an antenna array," *IEEE Transactions on Signal Processing*, vol. 67, no. 15, pp. 3885–3893, 2019.
- [5] M. Cui and L. Dai, "Channel estimation for extremely large-scale MIMO: Far-field or near-field?" *IEEE Transactions on Communications*, vol. 70, no. 4, pp. 2663–2677, 2022.

- [6] A. Guerra, F. Guidi, D. Dardari, and P. M. Djurić, "Near-field tracking with large antenna arrays: Fundamental limits and practical algorithms," *IEEE Transactions on Signal Processing*, vol. 69, pp. 5723–5738, 2021.
- [7] A. Kosasih, O. T. Demir, and E. Björnson, "Parametric near-field channel estimation for extremely large aperture arrays," in *The 57th Asilomar Conference on Signals, Systems, and Computers*, Pacific Grove, USA, 2023, pp. 162–166.
- [8] J. Liu, G. Yang, Y. Liu, and X. Zhou, "RIS empowered near-field covert communications," *IEEE Transactions on Wireless Communications*, vol. 23, no. 10, pp. 15 477–15 492, 2024.
- [9] H. Huang, M. F. Keskin, H. Wymeersch, X. Cai, L. Wu, J. Thunberg, and F. Tufvesson, "Hybrid precoder design for angle-of-departure estimation with limited-resolution phase shifters," *IEEE Transactions on Communications*, 2024 (Early Access).
- [10] X. Cai and W. Fan, "A complexity-efficient high resolution propagation parameter estimation algorithm for ultra-wideband large-scale uniform circular array," *IEEE Transactions on Communications*, vol. 67, no. 8, pp. 5862–5874, 2019.
- [11] X. Cai, W. Fan, X. Yin, and G. F. Pedersen, "Trajectory-aided maximum-likelihood algorithm for channel parameter estimation in ultrawideband large-scale arrays," *IEEE Transactions on Antennas and Propagation*, vol. 68, no. 10, pp. 7131–7143, 2020.
- [12] Z. Yuan, J. Zhang, Y. Ji, G. F. Pedersen, and W. Fan, "Spatial non-stationary near-field channel modeling and validation for massive MIMO systems," *IEEE Transactions on Antennas and Propagation*, vol. 71, no. 1, pp. 921–933, 2023.
- [13] M. Li, Z. Yuan, Y. Lyu, P. Kyösti, J. Zhang, and W. Fan, "Gigantic MIMO channel characterization: Challenges and enabling solutions," *IEEE Communications Magazine*, vol. 61, no. 10, pp. 140–146, 2023.
- [14] Y. Han, S. Jin, C.-K. Wen, and X. Ma, "Channel estimation for extremely large-scale massive MIMO systems," *IEEE Wireless Communications Letters*, vol. 9, no. 5, pp. 633–637, 2020.
- [15] J. Tian, Y. Han, S. Jin, and M. Matthaiou, "Low-overhead localization and VR identification for subarray-based ELAA systems," *IEEE Wireless Communications Letters*, vol. 12, no. 5, pp. 784–788, 2023.
- [16] H. Chen, P. Zheng, Y. Ge, A. Elzanaty, J. He, T. Y. Al-Naffouri, and H. Wymeersch, "ELAA near-field localization and sensing with partial blockage detection," in *IEEE 35th International Symposium on Personal, Indoor and Mobile Radio Communications (PIMRC)*, 2024, pp. 1–6.
- [17] Y. Chen and L. Dai, "Non-stationary channel estimation for extremely large-scale MIMO," *IEEE Transactions on Wireless Communications*, vol. 23, no. 7, pp. 7683–7697, 2024.
- [18] X. Zhang and J. Zheng, "Non-stationary near-field channel estimation for XL-MIMO systems with hybrid combining," *IEEE Wireless Communications Letters*, vol. 13, no. 10, pp. 2727–2731, 2024.
- [19] X. Cheng, K. Xu, J. Sun, and S. Li, "Adaptive grouping sparse Bayesian learning for channel estimation in non-stationary uplink massive MIMO systems," *IEEE Transactions on Wireless Communications*, vol. 18, no. 8, pp. 4184–4198, 2019.
- [20] H. Iimori, T. Takahashi, K. Ishibashi, G. T. F. de Abreu, D. González G., and O. Gonsa, "Joint activity and channel estimation for extra-large MIMO systems," *IEEE Transactions on Wireless Communications*, vol. 21, no. 9, pp. 7253–7270, 2022.
- [21] X. Tong, Z. Zhang, Y. Zhang, Z. Yang, C. Huang, K.-K. Wong, and M. Debbah, "Environment sensing considering the occlusion effect: A multi-view approach," *IEEE Transactions on Signal Processing*, vol. 70, pp. 3598–3615, 2022.
- [22] Y. Zhu, H. Guo, and V. K. N. Lau, "Bayesian channel estimation in multi-user massive MIMO with extremely large antenna array," *IEEE Transactions on Signal Processing*, vol. 69, pp. 5463–5478, 2021.
- [23] A. Tang, J.-B. Wang, Y. Pan, W. Zhang, X. Zhang, Y. Chen, H. Yu, and R. C. De Lamare, "Joint visibility region and channel estimation for extremely large-scale MIMO systems," *IEEE Transactions on Communications*, 2024.
- [24] W. Xu, A. Liu, M.-J. Zhao, and G. Caire, "Joint visibility region detection and channel estimation for XL-MIMO systems via alternating MAP," *IEEE Transactions on Signal Processing*, vol. 72, pp. 4827–4842, 2024.
- [25] C. M. Bishop, "Chapter 8.3 - Markov Random Fields," in *Pattern Recognition and Machine Learning*. Springer New York, NY, 2006, pp. 383–393.
- [26] 3GPP, "User equipment (UE) radio transmission and reception; Part 2: Range 2 Standalone," *3GPP TS 38.101-2: NR, Version 18.8.0, Release 18*, 2025. [Online]. Available: <https://portal.3gpp.org>